Co3O4, ZnO, Co3O4-ZnO Nanofibers and Their Properties

Kanjwal, Muzafar Ahmed; Sheikh, F. A.; Barakat, N. A. M.; Li, Xiaoqiang; Yong Kim, H.; Chronakis, Ioannis S.

Published in:
Journal of Nanoengineering and Nanomanufacturing

Link to article, DOI:
10.1166/jnan.2011.1016

Publication date:
2011

Document Version
Publisher's PDF, also known as Version of record

AMERICAN SCIENTIFIC PUBLISHERS

Journal of Nanoengineering and Nanomanufacturing
Vol. 1, pp. 196–202, 2011
(www.aspbs.com/jnan)

ARTICLE

Co_3O_4, ZnO, Co_3O_4-ZnO Nanofibers and Their Properties

Muzafar A. Kanjwal[1,*], Faheem A. Sheikh[2], Nasser A. M. Barakat[3], Xiaoqiang Li[1], Hak Yong Kim[3], and Ioannis S. Chronakis[1]

[1]*Technical University of Denmark, DTU Food, Soltofts plads, B 227, 2800 Kgs. Lyngby, Denmark*
[2]*Department of Chemistry, University of Texas Pan American, Edinburg, TX, 78539, USA*
[3]*Department of Textile Engineering, Chonbuk National University, Jeonju 561-756, Republic of Korea*

ABSTRACT

Coupled nanofibers consisting of cobalt oxide (Co_3O_4) and zinc oxide (ZnO) were prepared by the electrospinning process, and tested as a photocatalyst for dye degradation. Initially, electrospinning of a sol–gel consisting of cobalt acetate/zinc acetate/poly(vinyl alcohol) was used to produce polymeric nanofibers. Calcination of the obtained nanofibers in air at 600 °C produced (Co_3O_4-ZnO) nanofibers. Scanning electron microscopy (SEM), and transmission electron microscopy (TEM), were employed to characterize the as-spun nanofibers and the calcined product. X-ray powder diffractometery (XRD) analysis was also used to characterize the chemical composition and the crystallographic structure of the produced nanofibers. Photodegradation of rhodamine B (RB) dye was studied individually using three photocatalysts: (Co_3O_4-ZnO) nanofibers, pristine (Co_3O_4) and (ZnO) nanofibers. The (Co_3O_4-ZnO) nanofibers can eliminate all of the rhodamine B dye within about 90 min, however, the other two nanostructures could not totally eliminate all dye even after 3 h. Moreover, the tensile strength and the Young's modulus of coupled nanofibers were higher than that of pristine (CoAc/PVA) and (ZnAc/PVA) nanofibers. The increased mechanical properties of coupled nanofibers might be due to the chemical bonding between Zn^{2+} and Co^{2+}.

KEYWORDS: Cobalt Oxide, Zinc Oxide, Nanofibers, Photocatalyst, Mechanical Properties, Electrospinning.

1. INTRODUCTION

The use of different types of organic dyes and their intermediates in various industries such as plastics, paint, textiles, cosmetics and paper, pose a great hazard to the ambient ecosystem.[1] The removal of these colors and other organic compounds is a major concern in ensuring a safe and healthy environment, while the selection of appropriate materials to use for their removal is of considerable interest.[2] Due to versatile character of the transition metals, cobalt metal has many oxidation states and many oxide forms. Among the various oxide forms, cobalt(II) oxide (CoO) and cobalt(II, III) Co_3O_4 are especially studied because of their interesting properties. Co_3O_4 and its mixtures can be used as electrode materials in various applications such as reduction, electrochromic devices,[3,4] super capacitors,[5–7] lithium ion batteries,[8–11] protection film of cathodes in molten carbonate fuel cells,[12–14] oxygen evolution,[15–17] heterogeneous catalysis,[18–20] energy storage,[21] solid state sensors,[22,23] and as magnetic materials.[24] Both pure Co_3O_4 and coupled systems of Co_3O_4 with Al_2O_3, SiO_2, or TiO_2 were studied for the degradation of 2,4-dichlorophenol, however, the coupled systems show better degradation results.[25–28] It is to note as well that photocatalytic properties of metal oxides could be enhanced by coupling with other metal oxides.[29]

ZnO based nanomaterials have been intensively investigated because they are chemically stable and environmental friendly materials. Moreover, there is a great interest in studying ZnO in the form of single crystals, powders, nanostructures or thin films. ZnO has great potential for a variety of practical applications, such as optical waveguides, piezoelectric transducers, varistors, surface acoustic wave devices, phosphors, chemical and gas sensors, transparent conductive oxides, UV-light emitters, and spin functional devices.[30,31] ZnO has wide band gap of (3.37 eV),[30] and its high exciton-binding energy of (60 meV)[30] permits excellent excitonic emission even at room temperature, and thus it is considered as an interesting material for photonic applications.

Moreover, among the various one-dimensional (1D) nanostructure shapes, such as nanowires, nanorods, and nanofibers, the nanofibers have a specific advantage

*Author to whom correspondence should be addressed.
Email: muka@food.dtu.dk
Received: 30 September 2011
Accepted: 11 November 2011

due to their long axial ratios, as well as their high surface-to-volume ratios. These properties are essential for any catalyst in order to exhibit high photo catalytic activity. Nanofibers can be fabricated by many techniques such as interfacial polymerization,[32–33] electrochemical deposition,[34, 35] template-assisted,[36–38] seeding,[39] self-assembly[40–42] and electrospinning.[43–46] The electrospinning technique is the most widely utilized for the processing of metal oxide nanofibers.[47] In this study, we describe the novel synthesis of nanofibers composed of a mixture of two functional oxides (Co_3O_4–ZnO). Their photocatalytic activity for degradation of rhodamine B dye was compared with the activity of the individual (Co_3O_4) and (ZnO) nanofibers. The mechanical properties of both coupled and individual nanofibers were also investigated.

2. EXPERIMENTAL DETAILS

2.1. Materials

Zinc acetate dihydrate assay (99.0%) was obtained from Showa, Co. Japan. Poly vinyl alcohol (PVA) with a molecular weight (MW) of 65,000 g/mol was obtained from Dong Yang Chem. Co., South Korea. Cobalt(II) acetate tetra hydrate (CoAc) 98.0 assay was purchased from Junsei Co. Ltd., Japan. These materials were used without any further purification. Distilled water was used as the solvent.

2.2. Experimental Procedures

Different aqueous metal acetate solutions were prepared by dissolving each zinc acetate (ZnAc) and cobalt acetate (CoAc) in water at a ratio of 1:4. A sol–gel was prepared by mixing the obtained solutions with a PVA aqueous solution (10 wt%) at a ratio of 5:15. Typically, 1 g of each ZnAc and of CoAc were dissolved separately in 4 g of water and then mixed with 15 g of the PVA solution (10 wt%). Similarly, third type of solution was prepared by mixing 0.5 g of each ZnAc and CoAc with 4 g of water. The resultant solution was mixed with PVA solution at a ratio of 5:15. These mixtures were vigorously stirred at 50 °C for 5 h. The sol–gel was supplied through a plastic syringe attached to a capillary tip. A copper wire originating from the positive electrode (anode) was inserted into the sol–gel, and a negative electrode (cathode) was attached to a metallic collector covered with a polyethylene sheet. A voltage of 20 kV was applied to these solutions. The formed nanofiber mats were initially dried for 24 h at 80 °C under a vacuum and then calcined at 600 °C temperatures for 1 h in air with a heating rate of 2 °C/min.

The surface morphology of nanofibers was studied by using a JEOL JSM-5900 scanning electron microscope, JEOL Ltd, Japan, and a field-emission scanning electron microscope equipped with EDX (FE-SEM, Hitachi S-7400, Japan). The phase and crystallinity were characterized by using a Rigaku X-ray diffractometer (Rigaku Co., Japan) with Cu Kα ($\lambda = 1.54056$ Å) radiation over 2θ range of angles, from 20 to 80°. High-resolution images and selected area electron diffraction patterns were observed by a JEOL JEM 2010 transmission electron microscope (TEM) operating at 200 kV(JEOL Ltd, Japan). The concentration of the dyes during the photodegradation study was investigated by spectroscopic analysis using an HP 8453 UV-visible spectroscopy system (Germany). The spectra obtained were analyzed by the HP ChemiStation software 5890 Series. Using an instron mechanical tester (LLOYD instruments, LR5K plus, UK) in tensile mode, mechanical properties of the as-spun polymer fiber mats were measured. The specimen thicknesses were measured using a digital micrometer with a precision of 1 μm. The extension rate was 5 mm/min at room temperature and seven specimens with dimensions of 3.5 mm $\times$ 40 mm (width and length) were tested and averaged for each fiber mat. The surface composition was determined by a X-ray photoelectron spectroscopy analysis (XPS, AXIS-NOVA, Kratos Analytical Ltd, UK) using the following conditions: base pressure 6.5×10^{-9} Torr, resolution (pass energy) 20 eV and scan step 0.05 eV/step.

In this study, we used rhodamine B (RB) dye to investigate the photocatalytic activity of the synthesized coupled nanostructure, and its individual ingredients. The photocatalytic degradation of RB dye in the presence of pure Co_3O_4, ZnO and Co_3O_4-ZnO nanofibers was carried out in a simple photoreactor. The reactor was made of glass (1000-ml capacity, 23-cm height and 15-cm diameter), covered with alumina foil and equipped with an ultraviolet lamp emitting source at a 365 nm wavelength radiation. The initial dye solution and photocatalysts were placed in the reactor and continuously stirred until completely mixed during the photocatalytic reaction. Typically, 100 ml of dye solution (10 ppm, concentration) and 50 mg of catalyst were used. At specific time intervals, a 2-ml sample was withdrawn from the reactor and centrifuged to separate the residual nanofiber catalyst; then, the absorbance intensity was measured at the corresponding wavelength.[50]

3. RESULTS

The electrospinning technique utilizes the high voltage to charge superficial layer of a polymer solution and thus induces the expulsion of a liquid jet through a spinneret. The bending instability of jet promotes its stretch and subsequently, formation of ultra-thin fibers. Figures 1(a), (b) show SEM images of the dried electrospun nanofiber mats prepared from CoAc/PVA. Similarly, Figures 1(c)–(f) show SEM images of the dried ZnAc/PVA and CoAc/ZnAc/PVA, respectively. As shown in these figures the PVA polymer and acetates can be

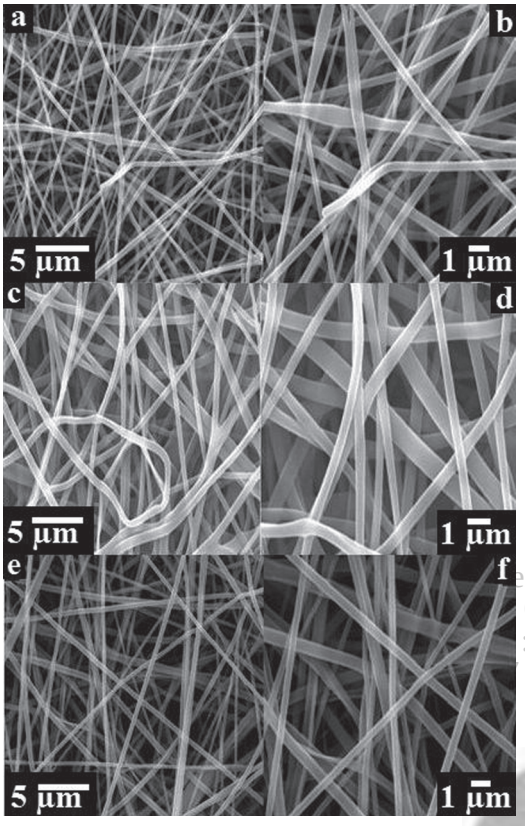

Fig. 1. Low and high magnification SEM images of the dried CoAc/PVA (a, b), ZnAc/PVA nanofibers (c, d) and CoAc/ZnAc/PVA (e, f).

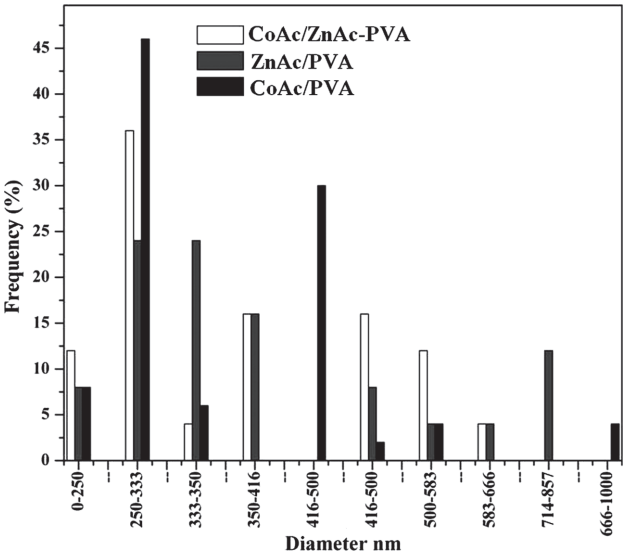

Fig. 2. Diameters frequency distribution curves for dried CoAc/PVA (a), ZnAc/PVA (b) and CoAc/ZnAc/PVA nanofibers (c).

electrospun to produce nanofibres of well defined morphology as there are no beads or agglomerated nanofibres observed in the obtained mats. Smooth and continuous nanofibers were formed by electrospinning technique of these sol–gels. It is to note also that the addition of different acetates did not affect the morphology of the nanofibers. Figure 2 shows the frequency curves of electrospun nanofibers. The average diameter of CoAc/PVA nanofibers was 426 nm, similarly with the average diameter of ZnAc/PVA and CoAc/ZnAc/PVA nanofibers (about 493 and 407 nm, respectively).

Figures 3(a), (b) show SEM images of nanofibers obtained after calcination of CoAc/PVA mats at 600 °C for 1 h. Similarly Figures 3(c)–(f) represent SEM images of nanofibers obtained after calcination of ZnAc/PVA and CoAc/ZnAc/PVA mats at 600 °C for 1 h, respectively. Obviously, this calcination temperature was adequate to obtain solid, continuous and smooth nanofibers. Moreover, it was found that the mixing of two different metal acetates has not affected the morphology of the calcined nanofibers.

Figure 4 shows the frequency curves of the nanofiber diameters after calcination. Calcination of all formulations resulted in a decrease in the average diameter of the calcined nanofibers in comparison to the electrospun one. According to these frequency distribution curves, the average diameters of the produced nanofibers were 186, 234, and 183 nm for Co_3O_4, ZnO, and Co_3O_4-ZnO nanofibers, respectively. The decreasing nanofiber diameter in all formulations can be explained by the removal of the polymer as a result of calcination at high temperature.

The crystal structures of the as-prepared different calcined nanofibers were examined by XRD (Fig. 5); note that spectra (a) refer to the calcined nanofibers and represents pure Co_3O_4 material. The apparent peaks at 2θ

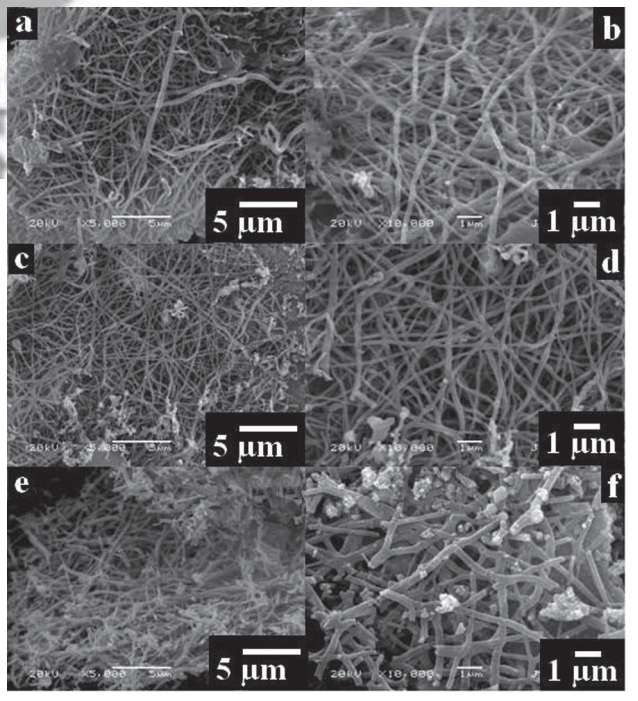

Fig. 3. Low and high magnification SEM images of the nanofibers obtained after calcination of the CoAc/PVA (a, b), ZnAc/PVA (c, d) and CoAc/ZnAc/PVA (e, f) at 600 °C for 1 h.

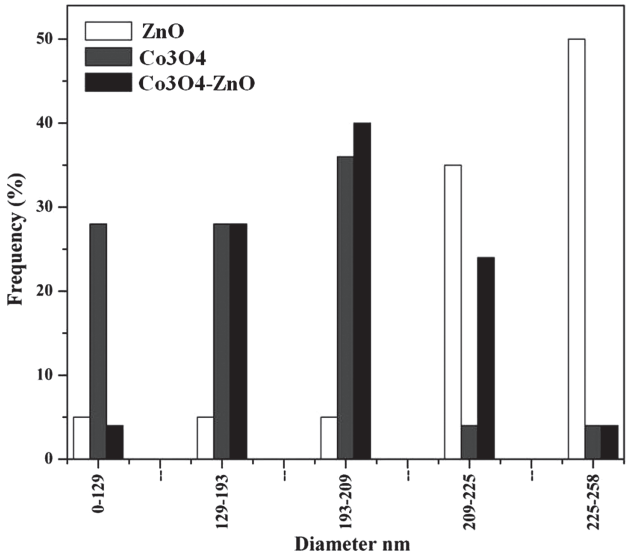

Fig. 4. Diameters frequency distribution curve for nanofibers obtained after calcination of the CoAc/PVA (a), ZnAc/PVA (b) and CoAc/ZnAc/PVA (c) nanofibers at 600 °C for 1 h.

values of 31.14, 36.58, 38.45, 44.68, 55.57, 59.30, 65.20 and 77.33° correspond to the crystal planes of (220), (311), (222), (400), (422), (511), (440) and (533), which confirms the formation of pure Co_3O_4 (JCPDS card No 42-1467). Similarly, the apparent peaks in the spectra (c) at 2θ values of 31.66, 34.22, 36.25, 47.86, 56.51, 62.66, 66.37, 67.92 and 69.26° correspond to the crystal planes of (100), (002), (101), (102), (110), (103), (200), (112), and (201), which confirms the formation of pure ZnO (JCPDS card No 36-1451). It is worth to mention here that spectra (b) which represents the calcined CoAc/ZnAc/PVA nanofibers at 600 °C for 1 h, contains both types of crystal peaks. Overall, the above results confirm the formation of (Co_3O_4–ZnO) nanofibers. To simplify the Figure 5, we have marked the peaks that correspond to cobalt oxide as (C) and to zinc dioxide as (Z).

X-ray photoelectron spectroscopy (XPS) analysis was also invoked to support the XRD data and to investigate the oxidation states, as well as the possible changes to the binding energies of the as-prepared calcined nanofibers. The samples for XPS were supported by carbon cloth electrodes, which are widely used in electrochemical experiments. No heat treatment on the samples was needed.

As shown at Figure 6, the peak at 284 eV that corresponds to the C 1s is expected, considering the graphite tape used during the sampling process. The Co 3p and 2p region in Co_3O_4 consists of the main 3p3/2 and 2p3/2 spin-orbit components with binding energies of 59 and 779 eV, respectively.[48] The Zn 2p region in ZnO consists of the main 2p3/2 and 2p1/2 spin-orbit components with binding energies of 1020 and 1043 eV, respectively. In addition to 2p, we also observed the 3d, 3p and 3s spin-orbit components for Zn at the binding energy of 10, 88 and 139 eV, respectively.[49] The 1s for oxygen is easily identified at a binding energy of 530 eV. Accordingly, XPS analysis affirmed that the synthesized material is consisting of (Co_3O_4–ZnO) nanofibers with good agreement with the XRD results.

The inner structure of the different synthesized nanofibers was studied by transmission electron microscopy (TEM), high-resolution transmission electron microscopy (HRTEM), and selected area electron diffraction pattern (SAED) analysis. TEM can be used to differentiate between the crystalline and amorphous structures. Moreover, it gives reliable information about the surface morphology. Structural characterization of the nanofibers that were prepared by calcination of CoAc/PVA is shown in Figures 7(a) and (b) (at low and high magnification, respectively). The high-resolution TEM image indicates good crystallinity since the atomic planes could be identified in 7(b). The SAED inset in 7(b) also indicates

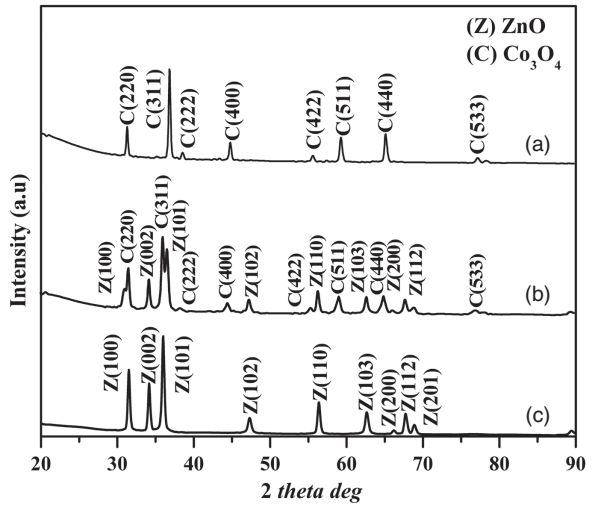

Fig. 5. XRD data for the nanofibers after calcination in the case of the CoAc/PVA (a), CoAc/ZnAc/PVA (b) and ZnAc/PVA (c) at 600 °C for 1 h.

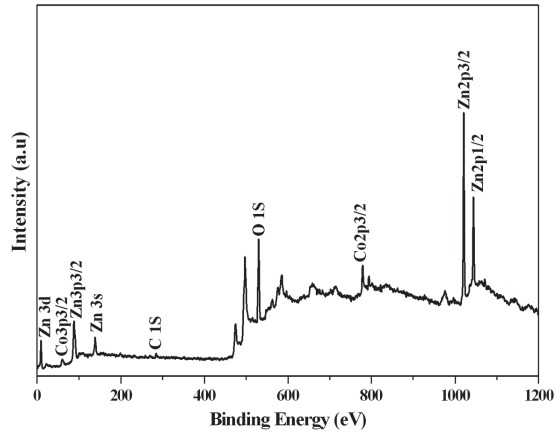

Fig. 6. XPS results for the nanofibers obtained from calcination of the CoAc/ZnAc/PVA nanofibers.

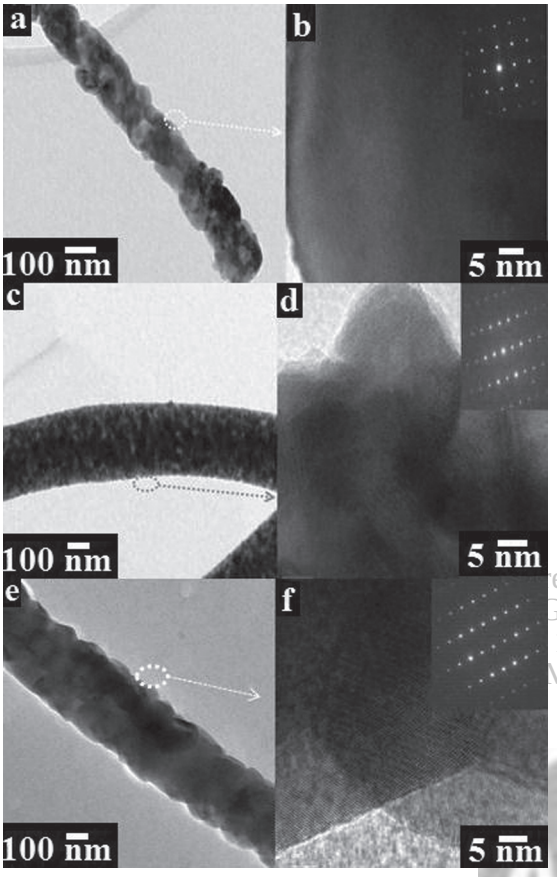

Fig. 7. TEM images at low and high magnifications for the nanofibers obtained from calcination of the CoAc/PVA (a, b), ZnAc/PVA (c, d) and CoAc/ZnAc/PVA (e, f). The insets in Figures (b, d and f) represent the corresponding high SAED patterns.

excellent crystalinity without dislocation and perforations. Moreover, Figures 7(c) and (d) show the low and high magnification TEM images of the calcined ZnAc/PVA nanofibers. The low magnification image of zinc oxide nanofibers shows smooth surfaces with clear borders, and without structural defects. Figure 7(d) shows the high-resolution TEM image of the marked area, in which the crystal planes are parallel with the same planar distance. The inset in 7(d) presents the SAED pattern of the same marked portion suggesting a good nanofiber crystalinity without any defects. Similarly, the TEM and HRTEM images along with the SAED patterns of the coupled (Co_3O_4–ZnO) nanofibers are shown in panels 7(e) and (f). Figure 7(e) shows the low magnification of (Co_3O_4–ZnO) nanofibers and is in agreement with the SEM image concerning the morphology and dimensions of these nanofibers. Figure 7(f) shows the high-resolution TEM image of the marked area, which indicates that the distance between two consecutive planes is the same and that the atomic planes are uniformly arranged in parallel, which indicates a good crystallinity. Moreover, different types of crystal planes with different distances between the successive planes can be observed in this figure, which might refer to the two oxides. It is worth to note here that the absence of any imperfection or dislocation in the SAED inset of Figure 7(f) confirms the good crystallinity of the synthesized nanofibers.

3.1. Applications

3.2. Mechanical Properties

To investigate the mechanical strength and toughness of fiber mats, tensile tests were conducted and their stress–strain curves were presented in Figure 8. The ultimate tensile strength (5.32 MPa) and percentage strain at maximum (66.37%) of the coupled (CoAc/ZnAc/PVA) nanofibers fiber mats were higher than those of CoAc/PVA nanofibers mats (tensile strength of 4.01 MPa and percentage strain at maximum 88.55%) and those of (ZnAc/PVA) nanofiber mats (4.32 MPa, 58.99%). Moreover, the (CoAc/ZnAc/PVA) nanofiber mat exhibits a higher Young's modulus (217 MPa) than those of the single acetate fiber mats. The Youngs modulus for (CoAc/PVA and ZnAc/PVA) was about (97 and 106 MPa), respectively. Hence, the Young's modulus of the coupled electrospun nanofiber was increased about 2 times, while the strain at break of the coupled nanofibers decreased, compared with that of the as-electrospun fiber mats. The improved mechanical properties of the coupled nanofibers could be due to the chemical bonding between Zn^{2+} and Co^{2+}. However, further specific studies are needed to investigate the mechanism of the improved tensile strength of coupled nanofibrous mats.

3.3. Photocatalytic Properties

Dye degradation is a common strategy to investigate the photocatalytic activity of various compounds. The degredation rate of RB without any catalyst was performed and

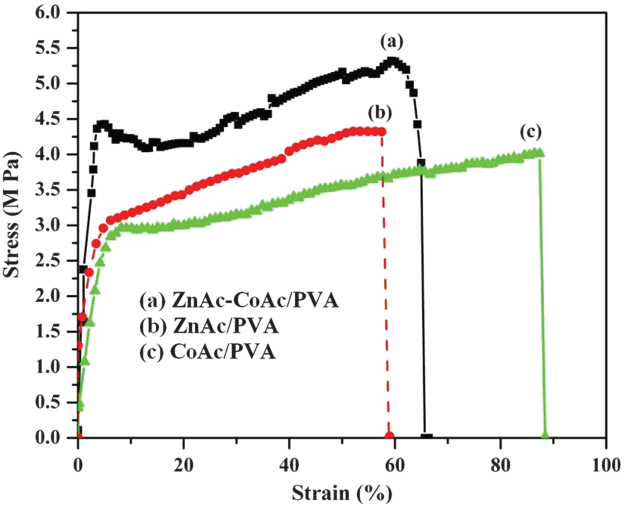

Fig. 8. Tensile stress–strain curve of pristine CoAc/ZnAcPVA (a), ZnAc/PVA (b) and CoAc/PVA nanofibers (c).

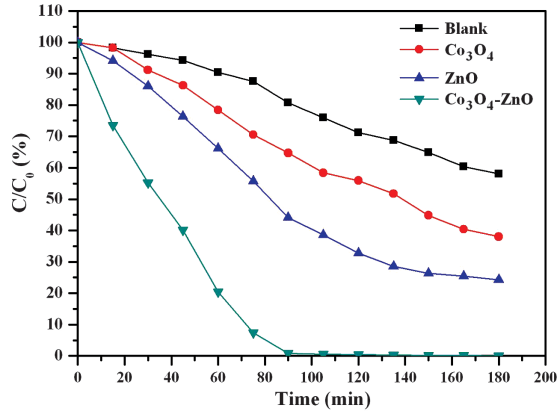

Fig. 9. Effect of blank, pristine (Co_3O_4), (ZnO) and (Co_3O_4/ZnO) nanofibers on the photocatalytic degradation of rhodamine B dye.

it could not help more than 40% even after 180 min, Significant increase in the degradation rate of RB dye was found using the coupled nanofibers (Fig. 9). In particular, within 60 min about 80% of the dye was degraded and completely eliminated after 90 min. This result could be due to synergetic coupling effect between (ZnO and Co_3O_4) and due to the high surface area of the nanofibers. However, in the case of pure ZnO nanofibers, almost 45% of the dye was oxidized after 60 min and all the dye could not be eliminated from the solution even after 3 h. Similarly, for pure Co_3O_4 nanofibers no more than 60% of the dye was oxidized even after 3 h.

The proposed mechanism for the enhanced photocatalytic activity of the Co_3O_4-ZnO nanostructure photocatalyst is attributed mainly to the coupling effect of Co_3O_4 and ZnO. Figure 10 shows the mechanistic scheme for charge separation and the photocatalytic reaction of (Co_3O_4-ZnO). The photo-generated electrons enter the conduction band of ZnO from that of the excited conduction band of Co_3O_4. Similarly, the photo- generated holes are also transferred from the valence band of ZnO to the valence band of Co_3O_4. This excellent charge separation enhances the lifetime of the charge carriers and enhances the efficiency of the interfacial charge transfer to

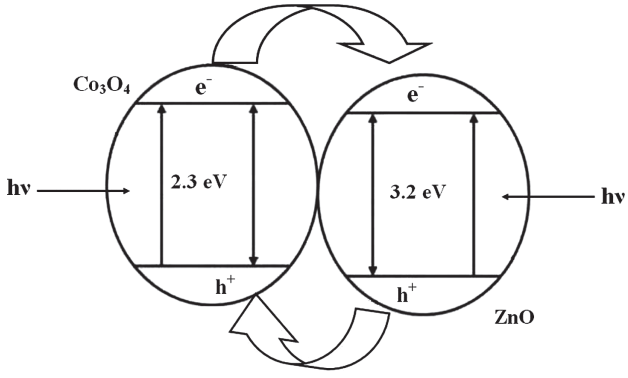

Fig. 10. A schematic diagram illustrating the principle of charge separation and photocatalytic activity for the (Co_3O_4-ZnO) system.

the adsorbed substrates. Thus, the photocatalytic properties are enhanced because the possibilities of recombination between photo-generated electrons and holes are reduced by facilitating their separation.

4. CONCLUSIONS

In this study, the electrospinning of (CoAc/PVA), (ZnAc/PVA) and (CoAc/ZnAc/PVA) nanofibers was reported. Calcination of the electrospun mats resulted in complete elimination of the polymer and production of Co_3O_4, ZnO and Co_3O_4-ZnO nanofibers with a uniform morphology. Scanning electron microscopy (SEM), and transmission electron microscopy (TEM), were employed to characterize the as-spun nanofibers and the calcined products. X-ray powder diffractometery (XRD) analysis was also used to study the chemical composition and the crystallographic structure of the produced nanofibers. Studies on the photodegradation of rhodamine B dye clearly reveal that the photocatalytic activity of the coupled nanofibers was higher than that of Co_3O_4 or ZnO individual nanofibers. Additionally, the (CoAc/ZnAc/PVA) nanofiber mats produced by this method exhibited a significant flexibility and improved mechanical properties. The tensile strength and the Young's modulus of the coupled nanofibers were higher than that of pristine (CoAc/PVA) and (ZnAc/PVA) nanofibers.

Acknowledgments: This work was supported by a grant from the Korean Ministry of Education, Science and Technology (The Regional Core Research Program/Center for Healthcare Technology and Development, Chonbuk National University, Jeonju 561-756 Republic of Korea). We thank Mr. T. S. Bae and J. C. Lim, KBSI, Jeonju branch, and Mr. Jong- Gyun Kang, Centre for University Research Facility, for taking the high-quality FE-SEM and TEM images, respectively.

References and Notes

1. F. Xia, E. Ou, L. Wang, and J. Wang, *Dyes Pigm.* 76, 76 **(2008)**.
2. M. A. Kanjwal, N. A. M. Barakat, F. A. Sheikh, S. J. Park, and H. Y. Kim, *Macromol. Res.* 18, 233 **(2010)**.
3. C. N. Polo da Fonseca, M. A. DePaoli, and A. Gorenstein, *AdV. Mater.* 3, 553 **(1991)**.
4. P. M. S. Monk and S. Ayub, *Solid State Ionics* 99, 115 **(1997)**.
5. C. C. Hu and C. Y. Cheng, *Electrochem. Solid-State Lett.* 5, A43 **(2002)**.
6. E. Hosono, S. Fujihara, I. Honma, M. Ichihara, and H. Zhou, *J. Power Sources* 158, 779 **(2006)**.
7. V. J. Srinivasan and W. Weidner, *J. Power Sources* 108, 15 **(2002)**.
8. D. Larcher, G. Sudant, J. B. Leriche, Y. Chabre, and J. M. Tarascon, *J. Electrochem. Soc.* 149, A234 **(2002)**.
9. G. Ceder, Y. M. Chiang, D. R. Sadoway, M. K. Aydinol, Y. I. Jang, and B. Huang, *Nature* 392, 694 **(1998)**.
10. H. Wang, Y. I. Jang, B. Huang, D. R. Sadoway, and Y. M. Chiang, *J. Electrochem. Soc.* 146, 473 **(1999)**.

ARTICLE

11. Y. Liu, C. Mi, L. Su, and X. Zhang, *Electrochim. Acta* 53, 2507 **(2008)**.
12. L. Mendoza, V. Albin, M. Cassir, and A. Galtayries, *J. Electroanal. Chem.* 548, 95 **(2003)**.
13. T. Pauporte, L. Mendoza, M. Cassir, M. C. Bernard, and J. Chivot, *J. Electrochem. Soc.* 152, C49 **(2005)**.
14. C. Mansour, T. Pauporte, A. Ringuede, V. Albin, and M. Cassir, *J. Power Sources* 156, 23 **(2006)**.
15. S. Trasatti, *Electrochim. Acta* 36, 225 **(1991)**.
16. Y. S. Lee, C. C. Hu, and T. C. Wen, *J. Electrochem. Soc.* 143, 1218 **(1996)**.
17. C. C. Hu and C. A. Chen, *J. Chin. Inst. Chem. Eng.* 30, 431 **(1999)**.
18. H. Kim, D. W. Park, H. C. Woo, and J. S. Chung, *Appl. Catal., B Environ.* 19, 233 **(1998)**.
19. D. Cao, J. Chao, L. Sun, and G. Wang, *J. Power Sources* 179, 87 **(2008)**.
20. A. Szegedi, M. Popova, V. Mavrodinova, and C. Minchev, *Appl. Catal. A* 338, 44 **(2008)**.
21. S. Noguchi and M. Mizuhashi, *Thin Solid Films* 77, 99 **(1981)**.
22. E. M. Logothesis, K. Park, A. H. Meitzler, and K. R. Laud, *Appl. Phys. Lett.* 26, 209 **(1975)**.
23. S. Abdollah, M. Hussein, H. Rahman, and S. Saied, *Sens. Actuators B* 129, 246 **(2008)**.
24. S. A. J. Makhlouf, *Magn. Mater.* 246, 184 **(2002)**.
25. W. Zhang, H. L. Tay, S. S. Lim, Y. Wang, Z. Zhong, and R. Xu, *Appl. Catal., B* 95, 93 **(2010)**.
26. Q. J. H. Choi, Y. J. Chen, and D. D. Dionysiou, *Appl. Catal. B* 77, 300 **(2008)**.
27. Q. J. Yang, H. Choi, and D. D. Dionysiou, *Appl. Catal. B* 74, 170 **(2007)**.
28. X. Y. Chen, J. W. Chen, X. L. Qiao, D. G. Wang, and X. Y. Cai, *Appl. Catal. B* 80, 116 **(2008)**.
29. M. A. Kanjwal, N. A. M. Barakat, F. A. Sheikh, and H. Y. Kim, *J. Mater. Sci.* 45, 1272 **(2010)**.
30. U. Ozgur, I. Alivov, C. Liu, A. Teke, M. A. Reshchikov, S. Dogan, V. Avrutin, S. J. Cho, and H. Morkoc, *J. Appl. Phys.* 98, 041301 **(2005)**.
31. R. Triboulet and J. Perriere, *Prog. Cryst. Growth Charact. Mater.* 47, 65 **(2003)**.
32. N. R. Chiou, C. Lu, J. J. Guan, L. J. Lee, and A. J. Epstein, *Nat. Nanotechnol.* 147, 354 **(2007)**.
33. R. Haggenmueller, F. Du, J. E. Fischer, and K. I. Winey, *Polymer* 47, 2381 **(2006)**.
34. Y. J. Yang, J. G. Zhao, and S. Hu, *Electrochem. Commun.* 9, 2681 **(2007)**.
35. H. Y. Yap, B. Ramaker, A. V. Sumant, and R. W. Carpick, *Diamond Relat. Mater.* 15, 1622 **(2006)**.
36. P. M. Ajayan, O. Stephan, P. Redlich, and C. Colliex, *Nature* 375, 769 **(1995)**.
37. M. Knez, *Nano Lett.* 3, 1079 **(2003)**.
38. N. V. Quy, N. D. Hoa, W. J. Yu, Y. S. Cho, G. S. Choi, and D. J. Kim, *Nanotechnology* 17, 2156 **(2006)**.
39. X. Y. Zhang, W. J. Goux, and S. K. Manohar, *J. Am. Chem. Soc.* 126, 4502 **(2004)**.
40. X. M. Yang, T. Y. Dai, Z. X. Zhu, and Y. Lu, *Polymer* 48, 4021 **(2007)**.
41. H. Hosseinkhania, M. Hosseinkhani, F. Tian, H. Kobayashi, and Y. Tabata, *Biomaterials* 27, 4079 **(2006)**.
42. J. D. Hartgerink, E. Beniash, and S. I. Stupp, *Science* 294, 1684 **(2001)**.
43. C. H. Kim, Y. H. Jung, H. Y. Kim, D. R. Lee, N. Dharmaraj, and K. E. Choi, *Macromol. Res.* 14, 59 **(2006)**.
44. Y. H. Jung, H. Y. Kim, D. R. Lee, S. Y. Park, and M. S. Khil, *Macromol. Res.* 13, 385 **(2005)**.
45. F. A. Sheikh, N. A. M. Barakat, M. A. Kanjwal, D. K. Park, S. J. Park, and H. Y. Kim, *Macromol. Res.* 18, 59 **(2009)**.
46. F. A. Sheikh, N. A. M. Barakat, M. A. Kanjwal, A. A. Chaudhari, J. I. Hee, J. H. Lee, and H. Y. Kim, *Macromol. Res.* 17, 688 **(2009)**.
47. W. Sigmund, J. Yuh, H. Park, V. Maneeratana, G. Pyrgiotakis, A. Daga, J. Taylor, and J. C. Nino, *J. Am. Ceram. Soc.* 89, 395 **(2006)**.
48. C. D. Wagner, J. F. Moulder, L. E. Davis, and W. M. Riggs, Perking-Elmer Corporation, Physical Electronics Division **(1982)**.
49. G. Ballerini, K. Ogle, and M. G. B. Labrousse, *Appl. Surf. Sci.* 253, 6860 **(2007)**.
50. M. A. Kanjwal, N. A. M. Barakat, F. A. Sheikh, M. S. Khil, and H. Y. Kim, *Int. J. Appl. Ceramic. Technol.* 7, E54 **(2010)**.